AUGUST 02 2004

Virtual sensing for broadband noise control in a lightly damped enclosure

Jing Yuan

J. Acoust. Soc. Am. 116, 934–941 (2004)
https://doi.org/10.1121/1.1768946

Virtual sensing for broadband noise control in a lightly damped enclosure

Jing Yuan[a)]
Department of Mechanical Engineering, The Hong Kong Polytechnic University, Hunghom, Kowloon, Hong Kong

(Received 17 July 2003; revised 6 March 2003; accepted 10 May 2004)

Available virtual sensing schemes either depend on assumptions that are valid for isolated frequencies, or require heavy online adaptations. A simple method is proposed here to predict the virtual signal exactly for broadband noise control in a lightly damped enclosure. The proposed method requires two physical sensors installed judiciously in a sound field to predict a virtual signal. The method is based on an exact mathematical relation between the virtual and physical sensors, which is valid for the entire frequency of interest. It is possible to use multiple sensor-pairs to reduce the sensitivity of the proposed method with respect to acoustic parameters, such as speed of sound or sensor mismatching. Experimental results are presented to verify the analytical results. © *2004 Acoustical Society of America.* [DOI: 10.1121/1.1768946]

PACS numbers: 43.50.Ki [KAC] Pages: 934–941

I. INTRODUCTION

In many active noise control (ANC) systems, secondary sources are employed to generate destructive interference and create local zones of quiet in sound fields.[1,2] Practical implementation of these systems requires the installation of error sensors in the quiet zones to monitor the ANC performance. In adaptive ANC systems, the adaptation of ANC transfer functions depends on the feedback of error signals.

In some applications, it may not be possible to install physical sensors in an area which is part of a quiet zone. Consequently sound signals in such an area have to be predicted with signals measured in other locations. The technique is known as virtual sensing, which was originated by Garcia-Bonito *et al.*[3,4] They make use of the fact that the spatial rate of pressure change of the primary field is small at low frequencies, and assumed that the primary field pressure is the same in both virtual and actual locations. They also observed that the pressure of the secondary source is different between the virtual and actual locations when both are close to the secondary source. The prior measurement of this difference makes it possible to estimate the signal at the virtual location. The method was applied to improve the performance of a pair of ANC ear defenders.[5] Another virtual sensing scheme is extrapolation of signals measured by physical sensors.[6] It was shown applicable to control tonal noise in the one-dimensional (1D) duct[7,8] and the three-dimensional (3D) free field.[9] For broadband applications, the extrapolation weights should be tuned by an adaptation algorithm.[10] Virtual sensors were also studied by Roure and Albarrazin,[11] assuming the existence of a transfer matrix $M(z)$ between the virtual signal vector $p_v(z)$ and the physical signal vector $p(z)$ via $p_v(z)=M(z)p(z)$.

Analytically, the relation between the virtual and physical signals is neither filtering nor extrapolating. Instead, it depends on both the primary and secondary sources. An exact way to predict the virtual signal is by means of an adaptive observer.[12] For virtual sensing of a tonal noise, an exact modal model of a sound field is required. If the model is truncated to the first m modes, then m online adaptive filters are required to adjust the observer state vector. If the noise contains multiple frequencies, the exact method[12] has an increased complexity proportional to the number of tonal frequencies.

For a noise field with a single broadband primary source, it is desired to have a simpler and exact virtual sensing method, which is proposed in this paper. This is an exact method based on the spatial distributions of the primary and secondary fields, and it is valid for the entire frequency range of interest. Only two physical sensors are required to predict a virtual signal exactly. Details of the proposed method are presented in the following text.

II. PRESSURE SIGNALS IN A DUCT

In most cases, available physical sensors are microphones measuring pressure signals. It is important to analyze the spatial distribution of pressure signals in a sound field, to design and implement an exact virtual sensing scheme. For this reason, a sound field in a lightly damped finite 1D duct is studied first.

A. A sound field in a finite 1D duct

Shown in Fig. 1(a) is a 1D ANC system, where the primary and secondary sources are placed at opposite ends of a duct. Let u_p, Z_p, u_s, and Z_s denote, respectively, the strengths and impedances of the sources where subscripts p and s refer to the primary and secondary sources. The strength of a mechanical-acoustic source is the volume velocity, and the strength of an electro-acoustic source is the driving current. Spatial distribution of sound signals may be described analytically by path transfer functions from the sources to a point x meters away from the primary source. The values of x are in the range $0 \leqslant x \leqslant l$ where l is the length of the duct.

[a)]Electronic mail: mmjyuan@polyu.edu.hk

 0001-4966/2004/116(2)/934/8/$20.00

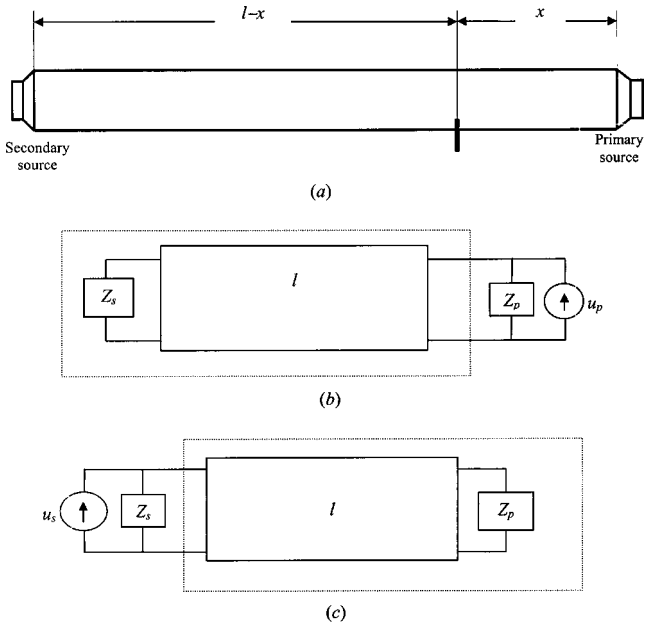

FIG. 1. (a) ANC configuration, (b) acoustic circuit of the primary field, and (c) acoustic circuit of the secondary field.

One way to obtain the path transfer functions is the use of transmission matrix, which is an exact model of 1D sound fields when the near field effects are negligible. The model is adopted here because the virtual sensor location can be assumed sufficiently away from noise sources. Let p_p and p_s denote, respectively, signals measured immediately in front of the two sources, when the secondary source is off ($u_s=0$), p_p and p_s, are related to each other by

$$\begin{bmatrix} p_p \\ v_p \end{bmatrix}_{u_s=0} = \begin{bmatrix} \cos(kl) & jZ_0\sin(kl) \\ j\dfrac{\sin(kl)}{Z_0} & \cos(kl) \end{bmatrix} \begin{bmatrix} p_s \\ \dfrac{p_s}{Z_s} \end{bmatrix}_{u_s=0}. \tag{1}$$

where Z_0 is the characteristic impedance of the duct; and v_p is the particle velocity caused by p_p. Equation (1) implies

$$\hat{Z}_s = Z_0 \frac{Z_s c_l + jZ_0 s_l}{Z_0 c_l + jZ_s s_l} = \left.\frac{p_p}{v_p}\right|_{u_s=0}, \tag{2}$$

where $c_l=\cos(kl)$, and $s_l=\sin(kl)$.

Impedance $\hat{Z}_s$ describes the acoustical effects of the dash-line box in Fig. 1(b), which acts as an acoustical load to the primary source when $u_s=0$. With the help of Eq. (2), one obtains

$$p_p|_{u_s=0} = \frac{\hat{Z}_s u_p}{Z_p+\hat{Z}_s} = \frac{Z_0(Z_s c_l + jZ_0 s_l)}{Z_0(Z_p+Z_s)c_l + j(Z_pZ_s+Z_0^2)s_l} u_p. \tag{3}$$

A microphone, placed x meters away from the primary source, measures signal p_x, which is related to p_p by

$$\begin{bmatrix} p_x \\ v_x \end{bmatrix}_{u_s=0} = \begin{bmatrix} c_x & -jZ_0 s_x \\ -j\dfrac{s_x}{Z_0} & c_x \end{bmatrix} \begin{bmatrix} p_p \\ \dfrac{p_p}{\hat{Z}_s} \end{bmatrix}_{u_s=0}, \tag{4}$$

where $c_x=\cos(kx)$ and $s_x=\sin(kx)$. Substituting Eq. (3) into Eq. (4), one obtains

$$p_x|_{u_s=0} = \frac{Z_0(Z_s c_{l-x} + jZ_0 s_{l-x})}{Z_0(Z_p+Z_s)c_l + j(Z_pZ_s+Z_0^2)s_l} u_p = H_{px}(j\omega)u_p, \tag{5}$$

where $c_{l-x}=\cos[k(l-x)]$, and $s_{l-x}=\sin[k(l-x)]$.

The derivation of secondary path $H_{sx}(j\omega)$ is very similar to that of $H_{px}(j\omega)$, due to the symmetric placement of the secondary source. Following a process similar to the derivation of Eq. (5), one can obtain

$$p_x|_{u_p=0} = \frac{Z_0(Z_p c_x + Z_0 s_x)}{Z_0(Z_p+Z_s)c_l + j(Z_pZ_s+Z_0^2)s_l} u_s = H_{sx}(j\omega)u_s. \tag{6}$$

One may combine Eqs. (5) and (6) to calculate the pressure at x from the primary source. The result is given by

$$p_x = Z_0 \frac{(Z_p c_x + jZ_0 s_x)u_s + (Z_s c_{l-x} + jZ_0 s_{l-x})u_p}{Z_0(Z_p+Z_s)c_l + j(Z_pZ_s+Z_0^2)s_l}, \tag{7}$$

which represents the spatial distribution of the field as a function of x, for the configuration of Fig. 1.

B. A novel virtual sensing scheme

Let p_1 and p_2 denote, respectively, signals measured by two physical sensors placed at x_1 and x_2. The objective is to predict p_v for a virtual sensor placed x_v meters away from the primary source. One may introduce a complex function

$$F(j\omega) = \frac{Z_0}{Z_0(Z_p+Z_s)c_l + j(Z_pZ_s+Z_0^2)s_l} \tag{8}$$

to represent the product of Z_0 with the denominator of Eq. (7). This makes it possible to rewrite Eq. (7) as

$$p_x = F(j\omega)[(Z_p c_x + jZ_0 s_x)u_s + (Z_s c_{l-x} + jZ_0 s_{l-x})u_p]. \tag{9}$$

Since $c_x=0.5(e^{jkx}+e^{-jkx})$ and $js_x=0.5(e^{jkx}-e^{-jkx})$, Eq. (9) is equivalent to

$$p_x = A(j\omega)e^{jkx} + B(j\omega)e^{-jkx}, \tag{10}$$

where

$$A(j\omega) = F(j\omega)\left[\frac{Z_p+Z_0}{2}u_s + \frac{Z_s-Z_0}{2}u_p e^{-jkl}\right] \tag{11a}$$

and

$$B(j\omega) = F(j\omega)\left[\frac{Z_p-Z_0}{2}u_s + \frac{Z_s+Z_0}{2}u_p e^{jkl}\right] \tag{11b}$$

are independent of x. These are the forward and backward waves traveling in the duct in opposite directions. For virtual sensing, Eq. (10) implies

$$\begin{bmatrix} p_1 \\ p_2 \end{bmatrix} = \begin{bmatrix} e^{jkx_1} & e^{-jkx_1} \\ e^{jkx_2} & e^{-jkx_2} \end{bmatrix} \begin{bmatrix} A(j\omega) \\ B(j\omega) \end{bmatrix} \tag{12}$$

and

$$\begin{bmatrix} A(j\omega) \\ B(j\omega) \end{bmatrix} = \frac{1}{e^{jx(x_1-x_2)} - e^{jk(x_2-x_1)}} \begin{bmatrix} e^{-jkx_2} & -e^{-jkx_1} \\ -e^{jkx_2} & e^{jkx_1} \end{bmatrix} \times \begin{bmatrix} p_1 \\ p_2 \end{bmatrix}. \quad (13)$$

The location of the virtual signal is in the range of $x_1 \geqslant x_v \geqslant x_2$. Once $A(j\omega)$ and $B(j\omega)$ are available, the virtual signal can be recovered exactly by $p_v = A(j\omega)e^{jkx_v} + B(j\omega)e^{-jkx_v}$.

C. Causality and accuracy

In a digital implementation, $\exp(-jkl) = \exp(-j\omega\tau)$ is equivalent to a delay time $\tau = l/c$, where c is the speed of sound. The implementation of $\exp(jkl) = \exp(j\omega\tau)$ is not causal, which is a practical problem if one wishes to predict a causal version of p_v. A possible solution is to rewrite Eq. (13) into

$$\begin{bmatrix} A(j\omega)e^{jkx_1} \\ B(j\omega)e^{-jkx_2} \end{bmatrix} = \frac{1}{1 - e^{2jk(x_2-x_1)}} \begin{bmatrix} 1 & -e^{jk(x_2-x_1)} \\ -e^{jk(x_2-x_1)} & 1 \end{bmatrix} \times \begin{bmatrix} p_1 \\ p_2 \end{bmatrix}, \quad (14)$$

where $A(j\omega)\exp(jkx_1)$ and $B(j\omega)\exp(-jkx_2)$ can be used to predict a causal version of $p_v = A(j\omega)e^{jkx_v} + B(j\omega)e^{-jkx_v}$ in the range of $x_1 \geqslant x_v \geqslant x_2$. It involves delay operations $\exp[jk(x_v - x_1)]$ and $\exp[jk(x_2 - x_v)]$, respectively. The implementation of Eq. (14) is causal because it contains a delay operator $\exp[jk(x_2 - x_1)]$. This method requires accurate knowledge of the speed of sound c.

Since the delay operator is equivalent to $\exp(-j\omega\tau_{12})$ with $\tau_{12} = (x_1 - x_2)/c$, an error δc in the speed of sound will cause an error in τ_{12}, denoted by $\delta\tau_{12} = (x_2 - x_1)\,\delta c/c^2$. One may reduce the distance between the two sensors to reduce the effect of $\delta\tau_{12} = (x_2 - x_1)\,\delta c/c^2$. A possible method is to place a pair of microphones in x_1 and $x_1' = x_1 - \Delta x$, respectively, to measure pressure signals p_1 and p_1'. A replacement of x_2 by $x_1' = x_1 - \Delta x$ in Eq. (14) leads to

$$\begin{bmatrix} A(j\omega)e^{jkx_1} \\ B(j\omega)e^{jk(\Delta x - x_1)} \end{bmatrix} = \frac{1}{1 - e^{-2jk\Delta x}} \begin{bmatrix} 1 & -e^{-jk\Delta x} \\ -e^{-jk\Delta x} & 1 \end{bmatrix} \times \begin{bmatrix} p_1 \\ p_1' \end{bmatrix}, \quad (15a)$$

where $A(j\omega)\exp(jkx_1)$ can be used to predict a causal version of p_v in the range of $x_1 \geqslant x_v \geqslant x_2$, by a simple delay operation $\exp[jk(x_v - x_1)]$. However, $B(j\omega)\exp[-jk(x_1 - \Delta x)]$ can only be used to predict p_v in the range of $x_1 \geqslant x_v \geqslant x_1 - \Delta x$. For this reason, another pair of sensors is placed in x_2 and $x_2 - \Delta x$, respectively, to measure pressure signals p_2 and p_2'. Replacing x_1 with x_2 in Eq. (15a), one obtains

$$\begin{bmatrix} A(j\omega)e^{jkx_2} \\ B(j\omega)e^{jk(\Delta x - x_x)} \end{bmatrix} = \frac{1}{1 - e^{-2jk\Delta x}} \begin{bmatrix} 1 & -e^{-jk\Delta x} \\ -e^{-jk\Delta x} & 1 \end{bmatrix} \times \begin{bmatrix} p_2 \\ p_2' \end{bmatrix}, \quad (15b)$$

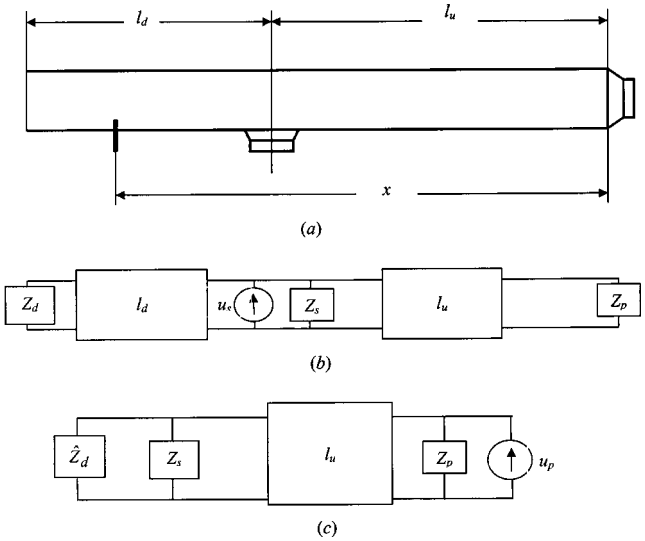

FIG. 2. (a) Another ANC configuration, (b) acoustic circuit of the secondary field, and (c) acoustic circuit of the primary field.

where $B(j\omega)\exp[jk(\Delta x - x_2)]$ can be used with $A(j\omega)\exp(jkx_1)$ to predict a causal version of $p_v = A(j\omega)e^{jkx_v} + B(j\omega)e^{-jkx_v}$ in the range of $x_1 \geqslant x_v \geqslant x_2$.

Theoretically, Eq. (14) is as exact as Eqs. (15a) and (15b). Both methods use delay operators equivalent to $\exp(-j\omega\tau_{12})$ and $\exp(-j\omega\Delta\tau)$, respectively, where $\tau_{12} = (x_1 - x_2)/c$ and $\Delta\tau = \Delta x/c$. If there is an error δc in the speed of sound, τ_{12} and $\Delta\tau$ contain errors $\delta\tau_{12}$ and $\delta\Delta\tau$, respectively. Since $\delta\tau_{12} = (x_2 - x_1)\,\delta c/c^2$ is significantly larger than $\delta\Delta\tau = \Delta x\,\delta c/c^2$ if $x_1 - x_2 \gg \Delta x$, the second method is less sensitive to errors in the speed of sound. Besides, the effect of possible sensor mismatch can be reduced by averaging the results obtained with multiple sensor-pairs.

III. A DIFFERENT CONFIGURATION

The ANC configuration in Fig. 1 is similar to those examined and tested by some researchers.[7,8,12] In many applications, the secondary source is placed between the primary source and the duct outlet as shown in Fig. 2. If virtual sensing is applied to such an ANC configuration, the proposed method must be modified.

A. Secondary path transfer function

The main difference between Figs. 1 and 2 is the location of the secondary source, which causes a different spatial distribution of the secondary field. The acoustical circuit for Fig. 2(a) is shown in Fig. 2(b) when the primary source is off. It is equivalent to a secondary source driving two parallel duct segments, though in reality this is a serial of up- and down-stream segments connected at the location of the secondary source.

The two segments of the duct are terminated by impedances Z_p and Z_d, respectively, where Z_p is the impedance of the primary source and Z_d is the impedance of the duct outlet. Similar to the derivation of Eq. (2), one can derive

$$\hat{Z}_p = Z_0 \frac{Z_p c_u + jZ_0 s_u}{Z_0 c_u + jZ_p s_u}, \quad \hat{Z}_d = Z_0 \frac{Z_d c_d + jZ_0 s_d}{Z_0 c_d + jZ_d s_d}, \quad (16)$$

where $c_u=\cos(kl_u)$, $s_u=\sin(kl_u)$, $c_d=\cos(kl_d)$, and $s_d=\sin(kl_d)$ respectively. Impedances $\hat{Z}_p$ and $\hat{Z}_d$ describe the loading effects of Z_p and Z_d to the secondary source. The parallel of $\hat{Z}_p$ and $\hat{Z}_d$ is $Z_1=\hat{Z}_d\hat{Z}_p/(\hat{Z}_d+\hat{Z}_p)$. The signal at the location of Z_1 is given by

$$p_s|_{u_p=0}=\frac{Z_1}{Z_s+Z_1}u_s=\frac{\hat{Z}_d\hat{Z}_p}{Z_s\hat{Z}_p+\hat{Z}_d(Z_s+\hat{Z}_p)}u_s. \tag{17}$$

Unlike the configuration of Fig. 1, a secondary path transfer function to a point x meters away from the primary source has two different expressions, depending on the values of x and l_u. For the case $x<l_u$, the secondary sound propagate upwards to reach x, which means

$$\begin{bmatrix} p_x \\ v_x \end{bmatrix}_{u_p=0}=\begin{bmatrix} \cos[k(l_u-x)] & -jZ_0\sin[k(l_u-x)] \\ -j\dfrac{\sin[k(l_u-x)]}{Z_0} & \cos[k(l_u-x)] \end{bmatrix} \times\begin{bmatrix} p_s \\ \dfrac{p_s}{\hat{Z}_p} \end{bmatrix}_{u_p=0}. \tag{18}$$

Let $c_{ux}=\cos[k(l_u-x)]$ and $s_{ux}=\sin[k(l_u-x)]$, then one can substitute Eq. (17) and write

$$p_x|_{u_p=0}=\frac{\hat{Z}_d(\hat{Z}_pc_{ux}-jZ_0s_{ux})}{Z_s\hat{Z}_p+\hat{Z}_d(Z_s+\hat{Z}_p)}u_s =G_u(\hat{Z}_pc_{ux}-jZ_0s_{ux})u_s, \tag{19}$$

where

$$G_u=\frac{\hat{Z}_d}{Z_s\hat{Z}_p+\hat{Z}_d(Z_s+\hat{Z}_p)}$$

is independent of x.

Similarly, for the case of $x\geqslant l_u$, the secondary sound propagate downwards to reach x, which means

$$\begin{bmatrix} p_x \\ v_x \end{bmatrix}_{u_p=0}=\begin{bmatrix} \cos[k(x-l_u)] & -jZ_0\sin[k(x-l_u)] \\ -j\dfrac{\sin[k(x-l_u)]}{Z_0} & \cos[k(x-l_u)] \end{bmatrix} \times\begin{bmatrix} p_s \\ \dfrac{p_s}{\hat{Z}_d} \end{bmatrix}_{u_p=0}. \tag{20}$$

Let $c_{xu}=\cos[k(x-l_u)]$ and $s_{xu}=\sin[k(x-l_u)]$, then one can use Eq. (17) again to write

$$p_x|_{u_p=0}=\frac{\hat{Z}_p(\hat{Z}_dc_{xu}-jZ_0s_{xu})}{Z_s\hat{Z}_p+\hat{Z}_d(Z_s+\hat{Z}_p)}u_s =G_d(\hat{Z}_dc_{xu}-jZ_0s_{xu})u_s, \tag{21}$$

where

$$G_d=\frac{\hat{Z}_p}{Z_s\hat{Z}_p+\hat{Z}_d(Z_s+\hat{Z}_p)}$$

is independent of x. Spatial distribution of the secondary field is now completely available as a function of x in Eq. (19) or Eq. (21), depending on the values of x and l_u.

B. Primary path transfer function

The transfer function of the primary path is derived by turning off the secondary source. As a result, the configuration of Fig. 2(a) is now represented by an acoustical circuit shown in Fig. 2(c). The down-stream segment, terminated by impedance Z_d, is equivalent to an impedance $\hat{Z}_d$ shown in the second equation of Eq. (16). The parallel of $\hat{Z}_d$ and Z_s is an impedance $Z_2=Z_s\hat{Z}_d/(Z_s+\hat{Z}_d)$, whose effects is an acoustical load to the primary source with an impedance

$$\hat{Z}_2=Z_0\frac{Z_2c_u+jZ_0s_u}{Z_0c_u+jZ_2s_u}. \tag{22}$$

Similar to the development of Sec. II, the pressure signal in front of the primary source is denoted by p_p, which is given by

$$p_p|_{u_s=0}=\frac{\hat{Z}_2u_p}{Z_p+\hat{Z}_2}, \tag{23}$$

when the secondary source is off.

The microphone sensor, placed x meters away from the primary source, measures pressure signal p_x, which is related to p_p by

$$\begin{bmatrix} p_x \\ v_x \end{bmatrix}_{u_s=0}=\begin{bmatrix} c_x & -jZ_0s_x \\ -j\dfrac{s_x}{Z_0} & c_x \end{bmatrix}\begin{bmatrix} p_p \\ \dfrac{p_p}{\hat{Z}_2} \end{bmatrix}, \tag{24}$$

where $c_x=\cos(kx)$ and $s_x=\sin(kx)$. Substituting Eq. (23) into the above equation, one obtains

$$p_x|_{u_s=0}=\frac{\hat{Z}_2c_x-jZ_0s_x}{Z_p+\hat{Z}_2}u_p=H_{px}(j\omega)u_p. \tag{25}$$

When both primary and secondary paths are available analytically, one can write

$$p_x=p_x|_{u_s=0}+p_x|_{u_p=0}=H_{px}(j\omega)u_p+H_{sx}(j\omega)u_s =\alpha(j\omega)e^{jkx}+\beta(j\omega)e^{-jkx}, \tag{26}$$

where

$$\alpha(j\omega)=\begin{cases} \dfrac{\hat{Z}_2-Z_0}{2(Z_p+\hat{Z}_2)}u_p+\dfrac{G_ue^{-jkl_u}}{2}(\hat{Z}_p+Z_0)u_s, & x<l_u \\ \dfrac{\hat{Z}_2-Z_0}{2(Z_p+\hat{Z}_2)}u_p+\dfrac{G_de^{-jkl_u}}{2}(\hat{Z}_d-Z_0)u_s, & x\geqslant l_u \end{cases} \tag{27a}$$

and

$$\beta(j\omega) = \begin{cases} \dfrac{\hat{Z}_2+Z_0}{2(Z_p+\hat{Z}_2)}u_p + \dfrac{G_u e^{jkl_u}}{2}(\hat{Z}_p-Z_0)u_s, & x<l_u \\ \dfrac{\hat{Z}_2+Z_0}{2(Z_p+\hat{Z}_2)}u_p + \dfrac{G_d e^{jkl_u}}{2}(\hat{Z}_d+Z_0)u_s, & x\geqslant l_u \end{cases} \tag{27b}$$

can be derived from Eqs. (19), (21), and (25). These two signals are independent of x, similar to $A(j\omega)$ and $B(j\omega)$ in Sec. II.

C. Modified scheme

Although $\alpha(j\omega)$ and $\beta(j\omega)$ look more complicated than $A(j\omega)$ and $B(j\omega)$ in Sec. II, the two signals need not be available analytically. Instead, they can be obtained from signals of the physical sensors. Since $\alpha(j\omega)$ and $\beta(j\omega)$ have different expressions in Eqs. (27a) and (27b), these signals need separate estimations for the case of $x<l_u$ and $x\geqslant l_u$, respectively. It means a double number of sensors and computation load.

One may reduce the number of sensors by separating the primary and secondary fields. In an ANC operation, the strength of the secondary source u_s is always available. It is also possible to identify a path transfer function $H_{sv}(j\omega)$ from offline data,[3–5,13,14] therefore $p_v|_{u_p=0}=H_{sv}(j\omega)u_s$ is available accurately. Only $p_v|_{u_s=0}$ needs prediction from signals p_1 and p_2. Before predicting $p_v|_{u_s=0}$, one may separate the primary field by

$$p_1|_{u_s=0}=p_1-H_{s1}(j\omega)u_s, \quad p_2|_{u_s=0}=p_2-H_{s2}(j\omega)u_s, \tag{28}$$

where $H_{s1}(j\omega)$ and $H_{s2}(j\omega)$ are transfer functions from the secondary source to the two physical sensors, available by offline identification.

Equation (25) describes the spatial distribution of the primary pressure field as a function of x. It may be expressed as

$$p_x|_{u_s=0}=\gamma(j\omega)e^{jkx}+\eta(j\omega)e^{-jkx}, \tag{29}$$

where

$$\gamma(j\omega)=\frac{\hat{Z}_2-Z_0}{2(Z_p+\hat{Z}_2)}u_p, \quad \eta(j\omega)=\frac{\hat{Z}_2+Z_0}{2(Z_p+\hat{Z}_2)}u_p$$

are valid in the entire duct. This implies

$$\begin{bmatrix} p_1 \\ p_2 \end{bmatrix}_{u_s=0} = \begin{bmatrix} p_1-H_{s1}u_s \\ p_2-H_{s2}u_s \end{bmatrix} = \begin{bmatrix} e^{jkx_1} & e^{-jkx_1} \\ e^{jkx_2} & e^{-jkx_2} \end{bmatrix} \begin{bmatrix} \gamma(j\omega) \\ \eta(j\omega) \end{bmatrix}, \tag{30}$$

and hence

$$\begin{bmatrix} \gamma(j\omega) \\ \eta(j\omega) \end{bmatrix} = \frac{1}{e^{jk(x_1-x_2)}-e^{jk(x_2-x_1)}} \begin{bmatrix} e^{-jkx_2} & -e^{jkx_1} \\ -e^{jkx_2} & e^{jkx_1} \end{bmatrix} \times \begin{bmatrix} p_1-H_{s1}u_s \\ p_2-H_{s2}u_s \end{bmatrix}, \tag{31}$$

which is very similar to Eq. (13). It can be re-written in a form similar to Eq. (14) for causal prediction of $p_v = \gamma(j\omega)e^{jkx_v}+\eta(j\omega)e^{-jkx_v}+H_{sv}(j\omega)u_s$, which requires the same number of sensors as Eq. (14) does.

IV. SOUND FIELD IN A 3D ENCLOSURE

Similar to the 1D case, locations of sources affect the spatial distributions of signals in a 3D sound field. Spatial relations between the virtual signal and physical signals may be descried analytically by path transfer functions between sources and sensors.

A. Path transfer functions

For a sound field in a lightly damped 3D enclosure, path transfer functions between sources and sensors may be modeled with the modal theory. The eigenfunctions of the sound field are denoted as $\phi_i(\mathbf{x})$ with spatial coordinate vector $\mathbf{x}$ and mode index $1\leqslant i\leqslant m$ for the first m modes. Let $\mathbf{x}_p$ and $\mathbf{x}_s$ represent spatial coordinates of the primary and secondary sources with strengths u_p and u_s, respectively. For a sensor placed at coordinate $\mathbf{x}$, the measured pressure signal is a linear superposition of two fields, with transfer functions given by

$$H_{px}(j\omega)=\left.\frac{p_x}{u_p}\right|_{u_s=0}=\sum_{i=1}^{m}\frac{\phi_i(\mathbf{x})\phi_i(\mathbf{x}_p)}{\omega_i^2-\omega^2+2j\xi_i\omega\omega_i} \tag{32}$$

and

$$H_{sx}(j\omega)=\left.\frac{p_x}{u_s}\right|_{u_p=0}=\sum_{i=1}^{m}\frac{\phi_i(\mathbf{x})\phi_i(\mathbf{x}_s)}{\omega_i^2-\omega^2+2j\xi_i\omega\omega_i}, \tag{33}$$

where ω_i and ξ_i are resonant frequency and damping ratio of the ith mode. In some applications, the primary source does not locate at a single spot $\mathbf{x}_p$. Let $w_p(\mathbf{x},t)$ model the primary source as a spatial and temporal function of $\mathbf{x}$ and t, then it may be expressed as $w_p(\mathbf{x},t)=f_p(\mathbf{x})u_p(t)$, where $f_p(\mathbf{x})$ describes the spatial distribution, $u_p(t)$ the temporal effect. One may rewrite Eq. (32) as

$$H_{px}(j\omega)=\left.\frac{p_x}{u_p}\right|_{u_s=0}=\sum_{i=1}^{m}\frac{\phi_i(\mathbf{x})f_i}{\omega_i^2-\omega^2+2j\xi_i\omega\omega_i}, \tag{34}$$

where $f_i=\int_X\phi_i(x)f_p(x)dx$ is the inner product of $f_p(\mathbf{x})$ with the ith eigenfunction of the noise field; and X represents the boundary of the sound field. Similar to the 1D fields, $H_{sx}(j\omega)$ and $H_{px}(j\omega)$ share the same denominator in a 3D resonant field. Their difference in the numerators is due to the different source locations $\mathbf{x}_p$ and $\mathbf{x}_s$, which vanishes if $\mathbf{x}_p=\mathbf{x}_s$.

In most ANC applications, digital controllers are implemented and path transfer functions are identified in the Z-transform domain as

$$H_{px}(z)=\left.\frac{p_x}{u_p}\right|_{u_s=0}=\frac{N_{px}(z)}{D(z)},$$

$$H_{sx}(z)=\left.\frac{p_x}{u_s}\right|_{u_p=0}=\frac{N_{sx}(z)}{D(z)}, \tag{35}$$

where all transfer functions share a same denominator $D(z)$; and they differ from each other in the numerators. The subscripts of the numerators indicate the source-destination of the paths.

B. Separation of primary and secondary signals

In this study, spatial coordinates of the two physical sensors and the virtual sensor are denoted as $\mathbf{x}_1$, $\mathbf{x}_2$, and $\mathbf{x}_v$, respectively. Transfer functions from the primary source to the two physical sensors and the virtual sensor are denoted, respectively, as $H_{p1}(z)$, $H_{p2}(z)$, and $H_{pv}(z)$; and transfer functions from the secondary source to the sensors are denoted as $H_{s1}(z)$, $H_{s2}(z)$, and $H_{sv}(z)$ respectively. These transfer functions are assumed available accurately by offline identification. Let p_1, p_2, and p_v denote, respectively, pressures of the two physical sensors and the virtual sensor, these signals are linear combinations of the primary and secondary fields, such as $p_1=H_{p1}(z)u_p+H_{s1}(z)u_s$. Due to the different spatial distributions of the primary and secondary fields, it is important to separate the two fields in predicting the virtual signal.

Since the strength of the secondary source is always available to the controller, it is relatively easy to predict the part of the virtual signal contributed by the secondary source. This part is simply $p_v|_{u_p=0}=H_{sv}(z)u_s$, where transfer function $H_{sv}(z)$ can be identified from offline measurement data. The focus is the prediction of the other part of the virtual signal, contributed by the primary source. For this reason, signals measured by the physical sensors should be processed first to remove the contributions of the secondary source by

$$p_1|_{u_s=0}=p_1-H_{s1}(z)u_s \tag{36}$$

before used to predict the virtual signal.

Some researchers used filters to recover a virtual signal from the signal of a physical sensor.[13,14] Let $F(z)$ denote the transfer function of such a filter, then broadband recovery of a virtual signal at location $\mathbf{x}_v$ is mathematically equivalent to

$$H_{pv}(z)=\frac{N_{pv}(z)}{D(z)}=H_{px}(z)F(z)=\frac{N_{px}(z)}{D(z)}F(z), \tag{37}$$

which requires

$$F(z)=\frac{N_{pv}(z)}{N_{px}(z)} \tag{38}$$

in a frequency range of interest.

In many ANC applications, path transfer functions are nonminimum phase, which means some roots of $N_{px}(z)$ are unstable and outside the unit circle in the Z plane. The filter in Eq. (38) is unstable in such a case, which is very likely to be true in an ANC application if the physical sensors do not collocate with the primary source.

C. The proposed method

The proposed method avoids Eq. (38) to avoid the instability of $N_{px}(z)$. It uses two physical sensors to predict a virtual signal. These sensors are installed judiciously in a noise field with coordinates $\mathbf{x}_1$ and $\mathbf{x}_2$, such that $N_{p1}(z)$ and $N_{p2}(z)$ do not share any zeros. This is ensured if the spectra of p_1 and p_2 do not have the same antiresonant frequencies, when both are measured in the absence of the secondary source.

When $N_{p1}(z)$ and $N_{p2}(z)$ do not share any zeros, there exist two polynomials $F_1(z)$ and $F_2(z)$, such that

$$N_{pv}(z)=N_{p1}(z)F_1(z)+N_{p2}(z)F_2(z), \tag{39}$$

which implies

$$H_{pv}(z)=H_{p1}(z)F_1(z)+H_{p2}(z)F_2(z). \tag{40}$$

Equation (39) is known as the Bezout equation,[15] which has a matrix-vector expression

$$\begin{bmatrix} n_{v0} \\ n_{v1} \\ \vdots \\ n_{vm} \end{bmatrix} = \begin{bmatrix} n_{10} & & & & n_{20} & & & \\ n_{11} & n_{10} & & n_{21} & n_{20} & & & \\ \vdots & n_{11} & \ddots & & \vdots & n_{21} & \ddots & \\ n_{1m} & & \ddots & n_{10} & n_{2m} & & \ddots & n_{20} \\ & n_{1m} & & n_{11} & & n_{2m} & & n_{21} \\ & & \ddots & \vdots & & & \ddots & \vdots \\ & & & n_{1m} & & & n_{2m} & \end{bmatrix} \times \begin{bmatrix} f_{10} \\ f_{11} \\ \vdots \\ f_{1m} \\ f_{20} \\ f_{21} \\ \vdots \\ f_{2m} \end{bmatrix}, \tag{41}$$

where $N_{pv}(z)=\Sigma_{i=0}^{m}n_{vi}z^{-i}$, $N_{p1}(z)=\Sigma_{i=0}^{m}n_{1i}z^{-i}$, $N_{p2}(z)=\Sigma_{i=0}^{m}n_{2i}z^{-i}$, $F_1(z)=\Sigma_{i=0}^{m}f_{1i}z^{-i}$, and $F_2(z)=\Sigma_{i=0}^{m}f_{2i}z^{-i}$, respectively. The matrix in Eq. (41) is known as the Sylvester resultant matrix, which is nonsingular if $N_{p1}(z)$ and $N_{p2}(z)$ do not share zeros.[15] This is ensured if the two physical sensors are installed judiciously.

The Bezout equation establishes the existence of the solutions in the entire frequency range of interest. It is valid when $N_{s1}(z)$ or $N_{s2}(z)$ is nonminimum phase. This is an important difference between the proposed method and those by Popovich[13] and Kammer.[14] Practically, $F_1(z)$ and $F_2(z)$ can be obtained adaptively, because the product of $u_p(z)$ to both sides of Eq. (40) leads to

$$\tilde{p}_v=F_1(z)\tilde{p}_1+F_2(z)\tilde{p}_2 \tag{42a}$$

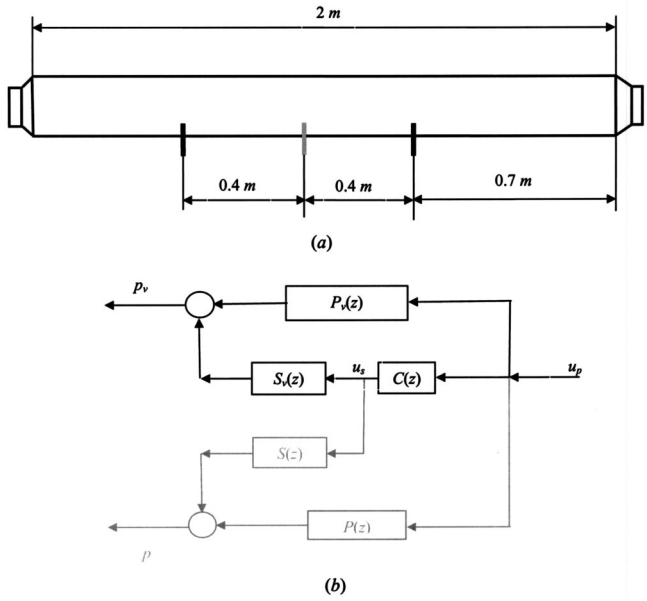

FIG. 3. (a) Experiment setup, (b) block diagram of the experiment system.

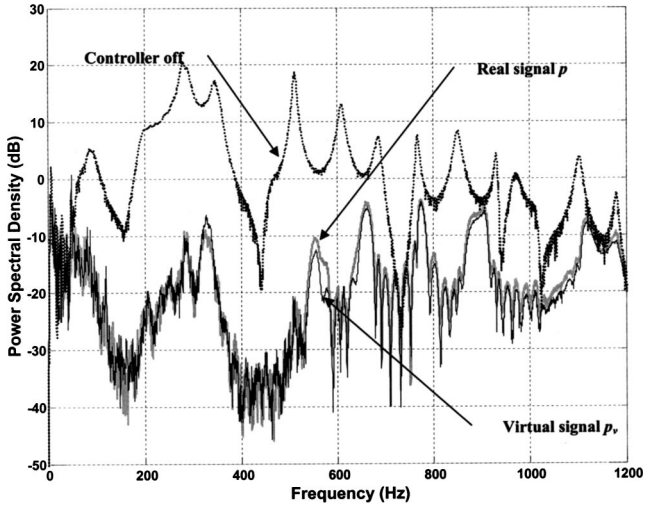

FIG. 4. Comparison of uncontrolled noise (dashed-black curve) with controlled real signal (thick-gray curve) and controlled virtual signal (thin-black curve).

where $\tilde{p}_v = H_{pv}(z)u_p$, $\tilde{p}_1 = H_{p1}(z)u_p$, and $\tilde{p}_2 = H_{p2}(z)u_p$ are measured when $u_s = 0$. The time domain version of Eq. (42a) is a regressive form

$$\tilde{p}_v(k) = \sum_{i=0}^{m} [f_{1i}\tilde{p}_1(k-i) + f_{2i}\tilde{p}_2(k-i)]. \tag{42b}$$

It may be used for the identification of $F_1(z)$ and $F_2(z)$ by a LMS algorithm when $u_s = 0$. Once $F_1(z)$ and $F_2(z)$ are available from Eq. (42b), the two polynomials are implemented as FIR filters to predict the virtual signal by

$$p_v = F_1(z)[p_1 - H_{s1}(z)u_s] + F_2(z)[p_2 - H_{s2}(z)u_s] + H_{sv}(z)u_s, \tag{43}$$

where $H_{s1}(z)$, $H_{s2}(z)$, and $H_{sv}(z)$ are available by offline identification.

V. EXPERIMENTAL VALIDATION

An experiment was conducted to verify the analytical results. A feedforward ANC was implemented in a duct with a cross-sectional area of $11 \times 14.5\ \text{cm}^2$ as depicted in Fig. 3(a). The primary and secondary actuators were 4 in loudspeakers placed at the opposite ends of the duct. Two physical sensors (represented by thick-black lines) were placed in the duct to predict the virtual sensor signal (represented by a thick-gray line). All sensor signals were low-pass filtered with a cutoff frequency 1 kHz.

A block diagram of the experimental system is shown in Fig. 3(b), where $P_v(z)$ and $S_v(z)$ represent the paths to the virtual sensor. The primary noise was a broadband pseudo-random signal. The virtual secondary path $S_v(z)$ was identified offline first, and then used by a filtered-x LMS ANC [not shown in Fig. 3(b) for brevity] to suppress virtual signal $p_v = A(j\omega)e^{jkx_v} + B(j\omega)e^{-jkx_v}$, where $A(j\omega)\exp(jkx_1)$ and $B(j\omega)\exp(-jkx_2)$ were calculated by substituting $x_1 = 1.5$ m and $x_2 = 0.7$ m into Eq. (14). The virtual signal p_v is supposed to predict the pressure signal p at $x_v = 1.1$ m with $x_1 \geqslant x_v \geqslant x_2$.

Since there may be implementation errors in the system, it is possible that the virtual signal p_v is well suppressed while the real signal p is not suppressed by the same amount. For this reason, a real sensor was placed at x_v to check the difference between p and p_v. The signal paths to the real sensor are depicted in Fig. 3(b) by the gray-lines, to show that these paths were not related to the control system.

The experimental results are plotted in Fig. 4 in three curves. The dashed-black curve, labeled "controller off," represents the normalized power spectral density (PSD) $|p(z)/u_p(z)|$ of the uncontrolled noise. The other curves were collected when the controller was active. The thick-gray curve, labeled "real signal p," plots the normalized PSD $|p(z)/u_p(z)|$. The thin-black curve, labeled "virtual signal p_v," represents the normalized PSD $|p_v(z)/u_p(z)|$. The difference between the two closely spaced curves are $|p(z)/u_p(z)|$ (real signal) versus $|p_v(z)/u_p(z)|$ (virtual signal).

The objective of the controller is to minimize $|p(z)/u_p(z)|$ without placing a real sensor at x_v. Since p was not available to the controller, the controller had to minimize $|p_v(z)/u_p(z)|$ without any information on p. The experiment verifies the effectiveness of the virtual sensor because the minimization of $|p_v(z)/u_p(z)|$ indeed leads to the minimization of $|p(z)/u_p(z)|$, though $|p_v(z)/u_p(z)|$ appears to be better than $|p(z)/u_p(z)|$ in some frequencies. Such a difference was due to implementation errors in the system.

Another way to verify the virtual sensing method is to compare p_v with either p_1 or p_2. For this reason, the primary and secondary sources were placed at the opposite ends of the duct. At convergence, the ANC created a quiet zone near x_v, which included neither x_1 nor x_2. Both p_1 and p_2 were collected in the experiment. Only p_1 is plotted in Fig. 5 to compare with p_v. Since p_1 was measured approximately halfway between the secondary source and x_v, its magnitude is significantly different from that of p_v, as shown in Fig. 5.

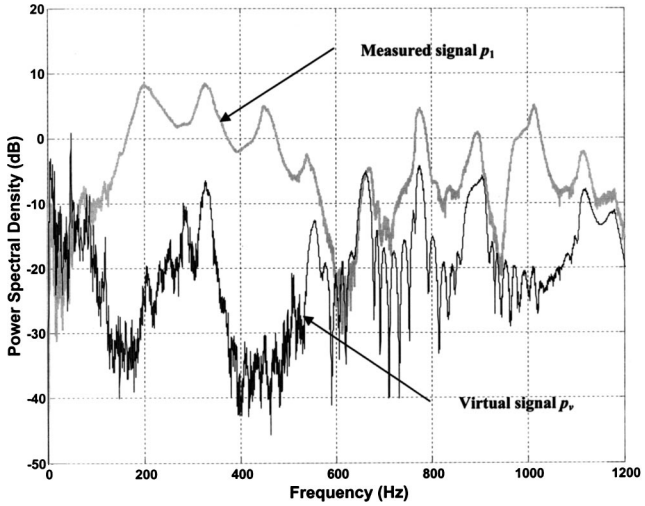

FIG. 5. Comparison of virtual signal p_v (thin-black curve) with a measured signal p_1 (thick-gray curve).

A similar difference exists between p_2 and p_v, since p_2 was measured between the primary source and x_v. That result is not plotted to avoid distractions due to the similar peak levels of p_1 and p_2 distributed in two sets of different frequencies.

VI. CONCLUSION

A novel virtual sensing scheme is developed for active control of broadband noise in lightly damped enclosures. It is based on path transfer functions derived analytically in sound fields. These transfer functions describe the analytical distribution of sound signals, on basis of which the proposed method is developed. Unlike available virtual sensing schemes, which work well for tonal signals, the proposed scheme enables exact prediction of the virtual signal in the entire frequency of interest. This method may be applied to an available ANC scheme for broadband noise control in a lightly damped field.

ACKNOWLEDGMENTS

The work described in this paper was substantially supported by a grant from the Research Grant Council of the Hong Kong Special Administration Region (Project No. PolyU 5175/01E).

[1] C. H. Hansen and S. D. Snyder, *Active Control of Noise and Vibration* (Spon, London, 1997).
[2] P. A. Nelson and S. J. Elliott, *Active Control of Sound* (Academic, London, 1992).
[3] J. Garcia-Bonito, S. J. Elliott, and C. C. Boucher, ''A virtual microphone arrangement in a practical active headrest,'' in Proceedings of Inter-noise, 96, pp. 1115–1120.
[4] J. Garcia-Bonito, S. J. Elliott, and C. C. Boucher, ''Generation of zones of quiet using a virtual microphone arrangement,'' J. Acoust. Soc. Am. **101**, 3498–3516 (1997).
[5] C. Carme and P. De Man, ''How to improve an ANC headset by using a virtual microphone,'' in Proceedings of Inter-noise, 98, Christchurch.
[6] B. S. Cazzolato, ''Sensing systems for active control of sound transmission into cavities,'' Ph.D. thesis, The University of Adelaide, Adelaide, South Australia, 1999.
[7] C. D. Kestell, B. S. Cazzolato, and C. H. Hansen, ''Active noise control with virtual sensors in a long narrow duct,'' Int. J. Acoust. Vibration **5**, 63–76 (2000).
[8] J. M. Munn, B. S. Cazzolato, C. D. Kestell, and C. H. Hansen, ''Virtual error sensing for active noise control in a one-dimensional waveguide: Performance prediction versus measurement,'' J. Acoust. Soc. Am. **113**, 35–38 (2003).
[9] C. D. Kestell, B. S. Cazzolato, and C. H. Hansen, ''Active noise control in a free field with virtual sensors,'' J. Acoust. Soc. Am. **109**, 232–243 (2001).
[10] B. S. Cazzolato, ''An adaptive LMS virtual microphone,'' in Proceedings of Active 2002, ISVR, Southampton, pp. 105–116.
[11] A. Roure and A. Albarrazin, ''The remote microphone technique for active noise control,'' in Proceedings of Active 1999, Ft. Lauderdale, FL, pp. 1233–1244.
[12] C. M. Tran and S. C. Southward, ''A virtual sensing method for tonal ANVC systems,'' ASME J. Dyn. Syst., Meas., Control **124**, 35–40 (2002).
[13] S. R. Popovich, ''Active acoustic control in remote regions,'' U.S. Patent, 5,701,350 (1997).
[14] D. C. Kammer, ''Estimation of structural response using remote sensor location,'' J. Guid. Control **20**, 501–508 (1997).
[15] G. C. Goodwin and K. S. Sin, *Adaptive Filtering, Prediction and Control* (Prentice–Hall, Englwood Cliffs, NJ. 1984).